A Shared Control Framework for Mobile Robots with Planning-Level Intention Prediction

Jinyu Zhang, Lijun Han, Member, IEEE, Feng Jian, Lingxi Zhang and Hesheng Wang, Senior Member, IEEE

Abstract-In mobile robot shared control, effectively understanding human motion intention is critical for seamless humanrobot collaboration. This paper presents a novel shared control framework featuring planning-level intention prediction. A path replanning algorithm is designed to adjust the robot's desired trajectory according to inferred human intentions. To represent future motion intentions, we introduce the concept of an intention domain, which serves as a constraint for path replanning. The intention-domain prediction and path replanning problems are jointly formulated as a Markov Decision Process and solved through deep reinforcement learning. In addition, a Voronoibased human trajectory generation algorithm is developed, allowing the model to be trained entirely in simulation without human participation or demonstration data. Extensive simulations and real-world user studies demonstrate that the proposed method significantly reduces operator workload and enhances safety, without compromising task efficiency compared with existing assistive teleoperation approaches.

Index Terms—mobile robot shared control, human intention prediction, deep reinforcement learning

I. INTRODUCTION

A. Motivation

MOBILE robots have advanced significantly in locomotion, perception, and navigation. However, they still struggle to handle demanding real-world tasks such as search and rescue. Their limitations in perception and cognitive awareness prevent them from adapting to complex and unpredictable environments. A promising direction to overcome these challenges is the integration of a human operator into the system, which is often referred to as a shared control framework. It leverages the complementary strengths of humans and robots: human adaptability and contextual awareness on one side, and robotic efficiency and precision on the other. As a result, system performance can be substantially improved.

In many tasks, mobile robots are expected to reach a target location or follow a predefined path. However, in practical missions, unforeseen events such as sudden environmental changes make it difficult to define these goals or trajectories beforehand. Consequently, human operators must guide the robot in real time, drawing on their experience and situational awareness. For effective collaboration, the robot must also act intelligently, adjusting its behavior according to the ongoing task and environmental cues. Therefore, how to best coordinate the two sources of intelligence from the human and the robot to ensure both safety and efficiency during task execution becomes a challenge.

To solve this problem, a common approach is to have the human operator directly decide the motion of the robot and convey his/her intention explicitly. Following this setup, several shared control frameworks have been proposed to blend human and autonomous inputs; for example, to help avoid collisions [1] or to provide assistive motion in a taskappropriate way [2]. However, commanding direct motion inputs requires a high commitment of the human, especially in complex tasks or cluttered environments.

To reduce this burden, other approaches extend shared control to the planning level. In this setting, the robot generates an initial trajectory using prior information before task execution. During operation, the robot continuously predicts human motion intentions and adjusts its desired trajectory accordingly. Therefore, when the trajectory aligns with the operator's intention, robot can move autonomously, effectively reducing the operator's workload. To implement this, [3] [4] rely on predefined models of user motion patterns and adjust the trajectory through deformation or replanning. However, due to the limited expressive capacity of explicit models, unmodeled human intentions may be ignored, thereby restricting robot control authority. To address this, [5] [6] capture motion patterns from the human demonstration data and generate the predicted trajectory in a receding-horizon fashion. Although these methods can capture the inherent multimodality of human actions, i.e. the possibility of multiple highly distinct futures, the generated trajectories often lack environmental constraints, making it difficult to guarantee safe robot operation.

Motivated by the limitations of existing shared control paradigms, we propose a novel mobile robot shared control framework with planning-level human intention prediction. In this framework, the human operator can not only intervene in the robot's current motion through a local shared controller but also modify the robot's desired path to influence its future motion plan. We proposed a path replanning algorithm to update the robot's desired path according to inferred human motion intentions, expressed as an intention domain. This domain is modeled as a conical region in two-dimensional space, encapsulating the likely area of the operator's intended movement over a short horizon. This representation enables the robot to infer short-term human goals while maintaining trajectory safety and efficiency. The proposed method integrates the reliability of rule-based planning with the flexibility of learning-based intention prediction. The algorithm performs replanning in two phases: in the first stage, it predicts the intention domain using contextual information and generates a trajectory segment within it. In the second stage, it completes the path by planning from the endpoint of the initial segment to the final task goal. We jointly model intention-domain prediction and path replanning as a Markov Decision Process, solved via deep reinforcement learning. A Voronoi-based trajectory generation algorithm is further developed to support learning entirely in simulation without requiring human participation or demonstration data.

B. Related Work

1) Mobile Robot Shared Control: Shared Control has played a major role in mobile robots as it has the potential to combine the strengths of human in global planning and coarse control and machine in fine motion control [7]. It has been widely used in the field of teleoperation [8] [9] [10] [11] [12] [13], operation of personal mobility platform [4] and co-transportation [5] [6] [14] [15]. For assisting the teleoperation of a mobile robot, a shared control law based on a hysteresis switch was proposed in [1] to guarantee the safety of the system without hitting any obstacles. To further reduce the operational and cognitive burden of humans, a bilateral shared framework was proposed in [8], where human operator allowed to modify online the shape of a planned path. In [9], a shared controller for Uncrewed Ground Vehicles (UGV) teleoperation was introduced, effectively deploying human robot shared control in the field. [10] developed a novel trilateral shared control architecture based on the velocity and force coordination of a dual-user haptic tele-training system for a hexapod robot. [11] and [12] have introduced a conavigation algorithm, where robot provides haptic guidance and path suggestions for both collision avoidance and guidance to a target. However, above approaches do not predict human intention during the task execution, which limits it to provide task-appropriate assistance to human operator.

2) Human Intention Prediction: In order to provide more useful assistance, researchers studying human-robot collaboration have dedicated significant effort to developing methods for human intention inference and action prediction. [16] divide relevant literature into three sections: inferring the human's intentions and goals, inferring specific collaborative features of the human, and predicting the human's future movement in space. The problem we focus on in this article can be considered as inferring the human's intentions and goals, that is, reasoning about the unobservable human goaloriented constructs that underlie their behavior. Reference [17] formulates a shared autonomy framework for robotic manipulators as a discrete-action partially observable Markov decision process (POMDP). The system predicts human grasping intentions and selects among goal-directed actions, nonassistive actions, and information-gathering actions to support effective collaboration. Reference [18] employs a fast randomized motion planner to generate multiple feasible motion plans as candidates for the predicted human intention and selects the best plan based on the energy function that includes human adjustment efforts. In [19], subgoals are extracted from human demonstration trajectories as a representation of user intention in hydraulic manipulator teleoperation. Based on this, an intention prediction based arbitration rule was established to blend the controllers of the human and robot. However, as we discussed earlier, above approaches have reduced intents to a selection of one of several goals or a limited numbers of

strategies, ignoring those unmodeled intents. To mitigate the shortage of explicit intention model, some researchers directly predict future human desired trajectory or actions in humanrobot collaboration. Authors in [20] developes a Gaussian Process Regression (GPR)-based approach to predict future human motions in a human-robot collaborative sawing task. The approach in [21] introduces a hybrid recurrent neural network to infer human motion intentions in collaborative assembly tasks, thereby enhancing interaction efficiency and coordination. Reference [22] proposed a learning-based model combining cascaded Long Short-Term Memory (LSTM) and Fully Connected (FC) layers to predict human desired trajectories in physical human-robot interaction. The approach in [23] predicts the human's force using a Deep Learning model in a Human-Robot collaborative object transportation task to improve human-robot interaction effectiveness. However, in practice, these method need extra low-level controller to guarantee the safety of predicted actions. Moreover, supervised learning method also relies on the quality of the available training data for accuracy, which are difficult to collect about humans, especially in specialized contexts like human-robot collaboration.

3) Human In the Loop Reinforcement Learning: Human in the loop reinforcement learning are a topic of active research. Integrating human inputs into learning process help agents to customize behavior and adapt to dynamic human needs, perceptions, and physical activities [24]. In many cases, it leverage human feedback to train autonomous agents, as a form of human-aided learning, to enhance the convergence rate and the quality of learned knowledge, e.g. the TAMER framework [25]. However, under shared control setting, the agent will always need cooperate with user to accomplish the task, due to the lack of the information that is private to the user and relevant to the task. Authors in [26] propose a deep reinforcement learning (DRL) framework for modelfree shared control. The success of assisting user in droneflying tasks illustrates the potential for DRL to enable flexible and practical assistive systems. In [27], authors train an agent cooperator in a real-world collaborative maze game using DRL. The study results show the existence of human-robot co-learning and the potential to tailor RL policies to human personalization. To leverage the power of simulation to train RL policies in human-involved task, Iterative-Sim-to-Real (i-S2R) was proposed in [28]. It bootstraps from a simple model of human behavior and alternates between training in simulation and deploying in the real world, refining both human behavior model and the policy. Inspired by these approaches, our work jointly addresses intention-domain prediction and path replanning within a unified deep reinforcement learning framework. To accelerate the training process, we further introduce a human trajectory generation algorithm that replaces real human operation, enabling model training to be conducted entirely in simulation.

C. Contributions

In this work, we present a novel shared control framework for mobile robots that incorporates planning-level human intention prediction. This framework enables humans and robots

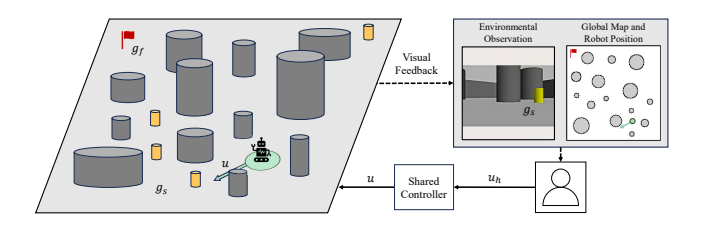


Fig. 1. System configuration.

to share the authority at both control and planning level in a flexible and safe manner.

The main contributions of this article are as follows.

- We introduce a closed-cone formulation of the intention domain and develop an intention-aware path replanning algorithm that leverages this representation to modify the robot's desired trajectory safely and efficiently.
- 2) We jointly learn both intention-domain prediction and path replanning policies using deep reinforcement learning. Additionally, a Voronoi-based human trajectory generation method is proposed to enable fully simulationbased training without requiring human data.
- 3) We conducted extensive experiments, including simulation studies on reward design, human in the loop simulations, and a real-world user study with ten participants. The results demonstrate that our method reduces operator workload and enhances safety without compromising task efficiency compared with existing assistive shared control approaches.

II. PROBLEM FORMULATION AND ALGORITHM OVERVIEW

A. Problem Formulation

The configuration of the system is shown in Fig. 1, where a human operator shares control with an autonomous mobile robot. The robot dynamics are defined as:

$$\begin{bmatrix} \dot{x} \\ \dot{y} \\ \dot{\theta} \end{bmatrix} = \begin{bmatrix} \cos \theta & 0 \\ \sin \theta & 0 \\ 0 & 1 \end{bmatrix} \begin{bmatrix} v \\ \omega \end{bmatrix} \tag{1}$$

where p=(x,y) denotes the Cartesian coordinates of the center of mass of the robot in the global reference frame and θ denotes the angular difference between the global and local reference frames. The control input $u=[v,\omega]$ consists of the forward velocity v and angular velocity ω , defined in the robot's local frame.

Similar to autonomous navigation, the task goal includes a final goal g_f , such as a supply station in a search-andrescue task. Beyond this, the task involves a set of sub-goals $\{g_s^1,\ldots,g_s^n\}$, which emerge during execution (e.g., victims detected during the mission). The human operator identifies these sub-goals through real-time environmental observation, such as the onboard camera view, and provides control inputs $u_h = [v_h, \omega_h]$ via an interface (e.g., joystick) to guide the robot toward them.

We assume that the robot has a prior map of the environment, represented as an occupancy grid, and can localize with respect to this map. Additionally, to support the operator's situational awareness, both the global map and the robot's current position are made available to the operator.

Problem definition: Given the system dynamics, a global map M, a final goal g_f , and a set of sub-goals $\{g_s^1,\ldots,g_s^n\}$, the human operator is required to guide the robot through all sub-goals before reaching the final goal. The operator has access to the global map, as well as the positions of the robot and the final goal, but the sub-goal locations are unknown in advance. Instead, the operator identifies sub-goals from environmental observations and provides control inputs $u_h = [v_h, \omega_h]$ to direct the robot toward them. The objective is to compute the robot's control input u such that task efficiency and safety are maintained while minimizing the operator's workload.

B. Algorithm Overview

The proposed shared control framework is illustrated in Fig. 2.

At the beginning of execution, the robot plans an initial path based on prior task knowledge and the global map, navigating autonomously toward the common goal. The current pose and planned path of the robot, global map, and onboard camera observations are presented visually to the operator.

When the current plan aligns with the operator's intent, the robot proceeds autonomously, thereby reducing the operational effort of the operator and allowing the operator to concentrate on higher-level situational awareness. However, when the operator intends to redirect the robot toward a subgoal, control commands u_r are issued through an interface. The shared controller integrates this command with contextual information to update system inputs u. At the same time, the planned path of the robot is adjusted accordingly. Once the revised path approaches the subgoal, as judged by the operator, the operator can return control authority to the robot.

To realize this interaction, we introduce a path replanning framework with intention domain prediction, enabling real-time and intention-aware path adaptation. Within this framework, a reinforcement learning (RL) agent is trained to determine the triggering policy for path replanning and, if triggered, to infer the corresponding intention domain. Furthermore, a shared control module implements a switching strategy: When the operator provides input, a modified shared dynamic window approach (DWA) controller generates safe control commands that align with human intent under kinematic and obstacle constraints; otherwise, a path-tracking controller computes inputs to keep the robot on its planned trajectory.

III. PATH REPLANNING ALGORITHM WITH INTENTION DOMAIN PREDICTION

A. Intention Domain

We propose the intention domain as a novel representation for predicting high-level human motion intentions in the shared control of mobile robots. Human intention is represented as a sequence of equally spaced points

$$\tau^h = [p_1^h, p_2^h, p_3^h, \dots, p_N^h] \in \mathbb{R}^{2N}$$
 (2)

where N is the number of points and the spacing Δd is determined by the grid map resolution. As we assume that

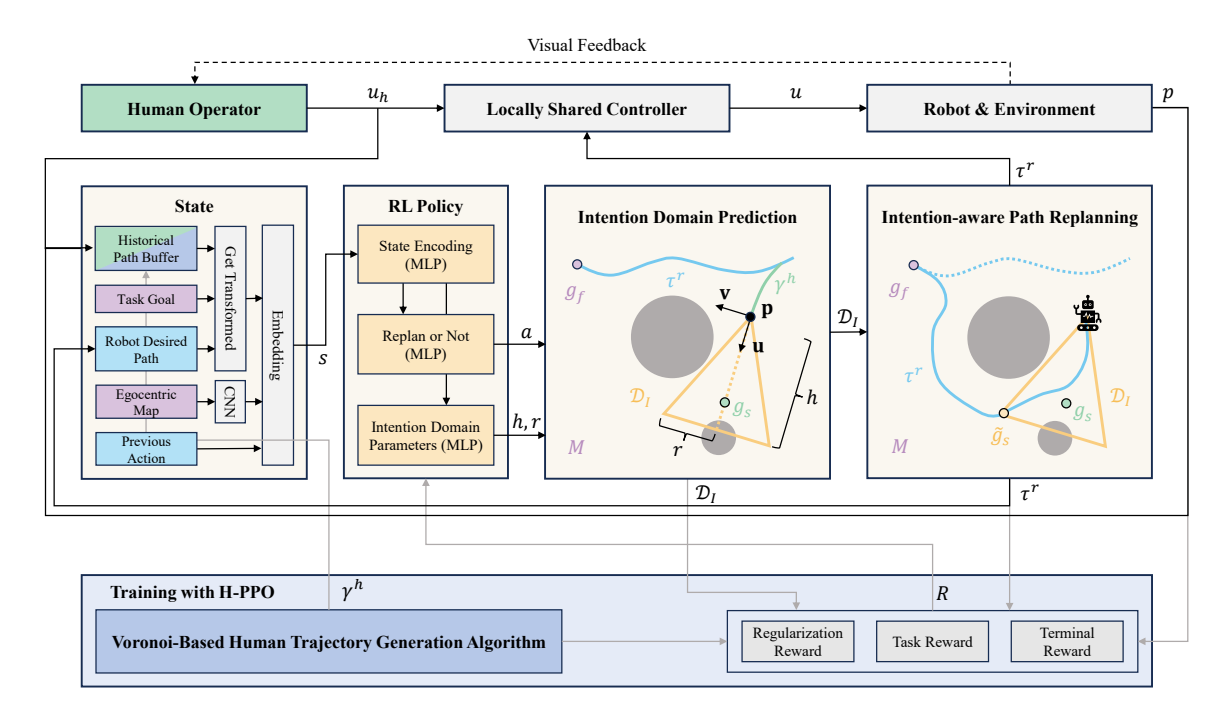


Fig. 2. The proposed shared control framework. Purple denotes environment and task priors, sky blue indicates robot intentions, green represents human motion intentions, and yellow shows inferred intentions in the form of an intention domain. Dark blue components correspond to modules used for policy training.

the robot tracks these points at maximum admissible velocity, higher-order motion information (e.g., velocity, acceleration) is excluded from this representation.

To predict future points, we adopt the paradigm of planning-based methods for human motion prediction [29]. These approaches model humans as rational agents, explicitly reasoning about long-term goals and computing policies to reach them. Similar to the rational human, the mobile robot in shared control also needs to generate an optimal path (e.g., minimizing distance or maximizing smoothness) to lead the operator toward the intended goal. However, planning-based prediction assumes predefined goals and generates optimal paths by reasoning over these goals. While effective for long-term planning, this assumption does not hold in shared control settings where sub-goals emerge dynamically.

To address this limitation, we introduce the concept of the intention domain. It is defined as a non-empty, connected, and closed set in \mathbb{R}^2 that contains the operator's future points. Intention prediction is thus decomposed into two steps: constraining the planning space to the predicted domain and generating points within it using planning-based reasoning.

As shown in Fig. 2, we assume that the intention domain \mathcal{D}_I is a closed (truncated) cone in \mathbb{R}^2 :

$$\mathcal{D}_I(\mathbf{p}, \mathbf{u}, h, r) = \{ x = \mathbf{p} + s\mathbf{u} + t\mathbf{v} \mid |t| \le \frac{r}{h}s, \ s \in [0, h] \}$$
(3)

where $\mathbf{p} \in \mathbb{R}^2$ is the apex, $\mathbf{u} \in \mathbb{R}^2$ is a unit vector along the cone axis and $\mathbf{v} \in \mathbb{R}^2$ is a unit vector perpendicular to u. The geometric parameters h and r represent the height and top radius of the cone, respectively. The half-opening angle is defined as $\phi = \arctan(\frac{r}{h}) \in [0, \frac{\pi}{2})$. As the human is modeled as a rational agent who rarely makes abrupt directional changes,

the predicted points are taken to extend forward from the robot's current position, following a direction closely aligned with the operator's current heading. Therefore, the intention domain is anchored at the robot's current position, while its axis direction u is derived from a sliding-window average of recent motion:

$$\mathbf{p} = p_0^h \\ \mathbf{u} = \frac{\sum_{i=1}^m (p_{1-i}^h - p_{-i}^h)}{\|\sum_{i=1}^m (p_{1-i}^h - p_{-i}^h)\|}$$
(4)

where $\{p_{-m}, \ldots, p_{-1}, p_0\}$ represents the robot's motion history during human intervention, stored in the historical path buffer γ^h . The buffer updates only when the user intervenes; otherwise, it is cleared. Each time the robot travels more than Δd , its current position is added to the buffer. The intention domain's geometric parameters, height h and radius r, are estimated from contextual information such as obstacle distribution and goal location. In this formulation, increasing h extends the temporal horizon of the prediction, while reducing the half-radius r constrains the predicted trajectory to remain more closely aligned with the operator's current heading.

In the following sections, we integrate this prediction process with path replanning, formulating the problem as a Markov Decision Process and solving it via deep reinforcement learning.

B. Intention-aware Path Replanning

When the human operator intervenes to direct the robot toward an sub-goal, the robot needs to generate a new trajectory that preserves safety while remaining consistent with human intention. Since the task is characterized by both transient sub-goals $\{g_s^1, ..., g_s^n\}$ and a final goal g_f , we distinguish

between short-term and long-term intentions. Accordingly, the proposed intention-aware path replanning algorithm consists of two stages: in the first stage, an intention domain is inferred from contextual cues, and a path segment τ^{rs} constrained to this domain is generated to capture short-term intent. In the second stage, a complementary segment τ^{rf} is planned to connect the first path to the final goal g_f and thereby fulfill the long-term task objective. The pseudo-code of the intentionaware path replanning algorithm is given in Alg. 1.

Algorithm 1 Intention-aware Path Replanning Algorithm.

Given:

```
• Control cycles: T, \delta
• Contextual information: M, g_f
 User-selected parameters: W, H^r, H^h
```

 $p \leftarrow \text{getRobotCurrentPosition}()$

Initialize:

end

```
\tau^r \leftarrow \text{pathPlanning}(p, g_f)
\gamma^h \leftarrow \emptyset
                                          > reset the histor buffer to empty
a \leftarrow 0
                     ▷ discrete action with 0: do nothing, 1: replan
every \delta seconds do
      p \leftarrow \text{getRobotCurrentPosition}()
      u^h \leftarrow \text{getHumanCmd}()
      \gamma^h \leftarrow \text{updateBuffer}(p, u^h)
      every T seconds do
            if humanInvolved(\gamma^h) then
                  M \leftarrow \text{getLocalMap}(p, M)
                  \tilde{g}_f, \tilde{\gamma}^h, \tilde{\tau}^r \leftarrow \text{getTransformed}(p, g_f, \gamma^h, \tau^r)
                  a, h, r \leftarrow \text{predictIntentionDomain}(\tilde{M}, \tilde{g}_f, \tilde{\gamma}^h, \tilde{\tau}^r, a)C. Reinforcement Learning Setup
            end if
            if a = 1 then
                  \mathcal{D}_I \leftarrow \text{getIntentionDomain}(\gamma^h, h, r)
                  \tilde{g}_s \leftarrow \text{getPredictedSubgoal}(\mathcal{D}_I, M, g_f)
                  \tau^{rs} \leftarrow \text{pathPlanning}(p, \tilde{q}_s) \triangleright \text{constrained to the}
intention domain
                  \tau^{rf} \leftarrow \text{pathPlanning}(\tilde{g}_s, g_f)
                  \tau^r \leftarrow \bar{\tau^{rs}} + \tau^{rf}
            end if
      end
```

The inputs of the algorithm consist of three parts:

- 1) **Control cycles**: the low-level control cycle δ determines the update rate of the robot's position and user commands, while the high-level decision cycle T determines the frequency of path replanning.
- 2) Contextual information: the occupancy grid map M and the final goal g_f .
- 3) User-selected parameters: the egocentric map width W, the observation length of robot intention H^r , and the buffer length of historical path points H^h

During initialization, a path from the robot's current position to the final goal g_f is planned with resolution Δd as the initial robot desired path, and the historical path buffer is empty. In

each control cycle δ , the buffer is updated according to the rules described in the previous subsection.

In each decision cycle T, the system first checks the buffer length to determine whether the user has influenced the robot's motion over a sufficiently long distance. If so, the path update process is triggered. Considering that when the robot desired path already passes near a sub-goal, the user's intervention may only indicate the desire for precise tracking rather than altering the entire future path. Thus, the update proceeds as follows: the first step is to decide whether replanning is necessary and, if so, to predict the geometric parameters of the intention domain. This decision is made by the reinforcement learning agent. The global occupancy map M is cropped into a egocentric map M centered on the robot's current position with width W. The final goal, the robot desired path, and the historical path buffer are all transformed into the robot's local coordinate frame. These contextual features, together with the last discrete action of the RL agent, serve as input to the policy network of the agent. The formulation of the RL problem and the process of policy training will be detailed in the next section.

If replanning is required, the intention domain is generated based on (3) and (4). Then, among the collision-free points on the base of the conical intention domain, the one closest to the final goal g_f is selected as the predicted sub-goal \tilde{g}_s . The first path segment τ^{rs} is planned from the robot's current position to this sub-goal, followed by the second segment τ^{rf} from the sub-goal to the final goal. At last, the two segments are concatenated to form the replanned trajectory.

To predict the intention domain containing the human desired path, we consider the problem of intention-aware path replanning as a single agent sequential decision-making problem. The human is seen as a part of the environment. We formalize the problem as a Markov Decision Process [30] consisting of a 4-tuple (S, A, R, f), whose elements are the state space S, action space A, reward function $R: S \times A \to \mathbb{R}$, and transition dynamics $f: \mathcal{S} \times \mathcal{A} \rightarrow \mathcal{S}$. An episode $(s_0, a_0, r_0, \ldots, s_n, a_n, r_n)$ is a finite sequence of $s \in \mathcal{S}$, $a \in \mathcal{A}, r \in \mathcal{R}$ elements, beginning with a start state s_0 and ending when the environment terminates. We define a parameterized policy $\pi_{\theta}: \mathcal{S} \to \mathcal{A}$ with parameters θ . The objective is to maximize $\mathbb{E}\left[\sum_{t=1}^{N} r(s_t, \pi_{\theta}(s_t))\right]$, the expected cumulative reward obtained in an episode under π_{θ} .

The state space in our reinforcement learning formulation consists of five structured components: (i) a local cost map M, cropped with width W around the robot's current position; (ii) the final goal \tilde{g}_f , represented in the robot's local frame; (iii) the robot's desired path segment $\tilde{\tau}^r$ of length H^r ; (iv) a historical path buffer $\tilde{\gamma}^h$ containing H^h past points; and (v) the most recent action type a. The trajectory segment $\tilde{\tau}^r$ is extracted from the robot planned path τ^r by locating the point that is closest to the robot's current position and sampling H^r subsequent points from it. Human intervention is explicitly captured in the historical path buffer $\tilde{\gamma}^h$ and implicitly reflected in \tilde{M} , \tilde{g}_f , and $\tilde{\tau}^r$ due to their transformation into the robot's coordinate frame. The action space is a parameterized action space. Following notation in [31], a complete action is represented as a tuple (a, x_a) , where $a \in \mathcal{A}_d$ is the discrete action and $x_a \in \mathcal{X}_a$ is the parameter to execute with action a. The whole action space \mathcal{A} is then the union of each discrete action with all possible parameters for that action:

$$\mathcal{A} = \bigcup_{a \in \mathcal{A}_a} \{ (a, x_a) \mid x_a \in \mathcal{X}_a \}. \tag{5}$$

In our problem, the discrete action decides whether to trigger path replanning. The parameter of not triggering is none set; while the parameter of triggering is the height h and top radius r of the intention domain. The details of the training process and reward structure are elaborated in the next section.

One algorithm for solving this problem is the hybrid proximal policy optimization (H-PPO) [32]. It takes a hybrid actorcritic architecture and uses PPO as the policy optimization method. PPO is a state-of-the-art policy optimization method that learns a stochastic policy π_{θ} by minimizing a clipped surrogate objective [33] as

$$L^{CLIP}(\theta) = \hat{\mathbb{E}}_t[\min(r_t(\theta)\hat{A}_t, \operatorname{clip}(r_t(\theta), 1 - \epsilon, 1 + \epsilon)\hat{A}_t)]$$

$$r_t(\theta) = \frac{\pi_{\theta}(a_t|s_t)}{\pi_{\theta_{old}}(a_t|s_t)}$$
(6)

where $r_t(\theta)$ denotes the probability ratio and ϵ is a hyperparameter. The hybrid actor-critic architecture used in our problem consists of two parallel actor networks and a critic network. The parallel actors perform action-selection and parameter-selection separately. The critic network works as an estimator of the state-value function V(s) to avoid the overparameterization problem in parameterized action space.

D. Training with Human Trajectory Generation

As shown in Alg. 1, the intention-aware path replanning module is triggered only when the human intervenes to adjust the robot's motion. However, training such a policy directly with human participation is impractical, as the limited sampling efficiency of reinforcement learning would lead to prohibitively long training times. To overcome this challenge, we propose a Voronoi-based trajectory generation algorithm that synthesizes human-like trajectories online. This approach eliminates the need for human involvement during training and substantially improves training efficiency.

As discussed earlier, even when the start and end positions are specified, the existence of sub-goals yields multiple possible trajectories. Therefore, we classify this trajectory uncertainty into global uncertainty and local uncertainty.

Global uncertainty arises from the trajectory's topological relation to obstacles. For example, a human navigating around an obstacle may choose either the left or the right side. This form of uncertainty is naturally captured by homotopically distinct trajectories [34], which we model using Voronoi graphs. Local uncertainty stems from unknown sub-goal positions and the variability of human control. To capture it, we extend the concept of flight corridors [35]. Specifically, we build a corridor sequence composed of circles aligned with Voronoi edges, then sample via-points within each circle. Finally, a trajectory planner generate human-like trajectories by jointly considering

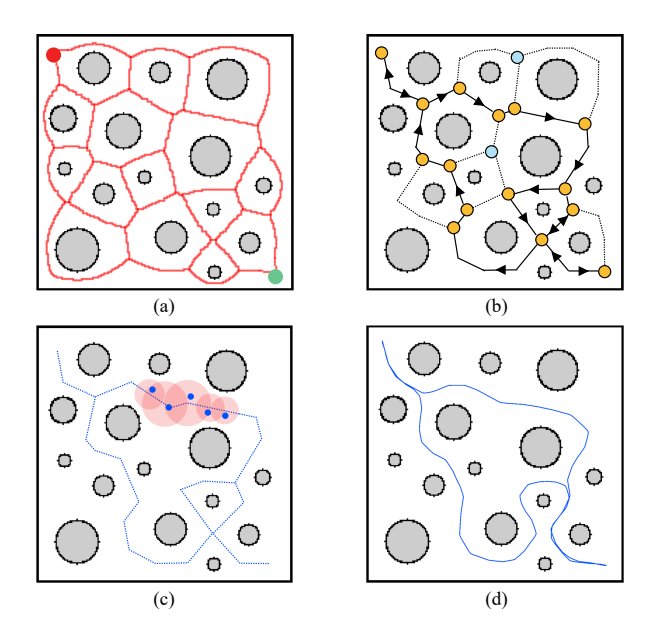


Fig. 3. Voronoi-based human trajectory generation algorithm: (a) Extracte the Discretized Voronoi Diagram (DVD) from the occupancy grid map. The start and goal are denoted by the green and red points. (b) Convert DVD into a Voronoi Graph. The sampled points are indicated by yellow nodes. (c) Generate initial trajectory along the Voronoi Graph edges, construct circular corridors and sample via-points within each corridor. (d) Trajectory planning under both corridor and via-point constraints

obstacles, via-points, and the robot's kinematic constraints. The pseudo-code of the human trajectory generating algorithm is given in Alg. 2.

As shown in Fig. 3 (a), the algorithm begins by converting the global occupancy grid into a Discretized Voronoi Diagram (DVD) [36], defined as the set of points equidistant from at least two obstacles. Following [37], the DVD is then converted into a Voronoi Graph consisting of nodes and edges, constructed with respect to the given start and goal positions. Edges that are too narrow for the robot to safely pass through are discarded. Since paths belonging to different homotopy classes may share common edges, we restrict sampling to simple paths from the Voronoi Graph. Furthermore, to model trajectory segments where the operator may temporarily move away from the global goal during sub-goal exploration, we sample a loop path by connecting a simple path sampled from the goal to the start with another path from the start to the goal, as illustrated in Fig. 3(b). Paths are sampled using a probabilistic depth-first search, selecting the next unvisited node uniformly and applying backtracking when necessary, thereby favoring shorter trajectories. For each sampled path, an initial trajectory is generated along the corresponding Voronoi edges. Circular corridors are then constructed around successive path points, where the radius equals the minimum distance from obstacles minus the robot radius. The center of the next circle is defined as the first path point outside the current circle. Within each corridor, a two-dimensional Gaussian distribution, parameterized by the circle center and radius, is used to sample via-points, as shown in Fig. 3(c). Finally, the Timed Elastic Band (TEB) trajectory planning algorithm [38] is used to generate the human-like trajectory.

At the start of each training episode, a human trajectory

Algorithm 2 Voronoi-based Human Trajectory Generation.

• Start and end points: p_{start} , p_{end}

Given:

 \bullet Global map: M

```
Control cycle: \delta
Initialize:
M_v \leftarrow \text{getDiscretizedVoronoiDiagram}(M)
G \leftarrow \text{buildVoronoiDiagram}(M_v, p_{start}, p_{end})
V_s \leftarrow \text{getStartNode}(G)
V_e \leftarrow \text{getEndNode}(G)
S \leftarrow \emptyset
                                  be the set of nodes on a simple path
S.\mathsf{pushBack}(V_e)
V_{next} \leftarrow \text{sampleNeighbors}(G, V_e)
while V_{next} \neq V_s do
     S.pushBack(V_{next})
     if hasNoValidNeighbor(G, V_{next}) then
           V_{next} \leftarrow \text{backTracking}(G, S)
     V_{next} \leftarrow \text{sampleNeighbors}(G, V_{next})
end while
S.pushBack(V_s)
V_{next} \leftarrow \text{sampleNeighbors}(G, V_s)
while V_{next} \neq V_e do
     S.\mathsf{pushBack}(V_{next})
     if hasNoValidNeighbor(G, V_{next}) then
           V_{next} \leftarrow \text{backTracking}(G, S)
     V_{next} \leftarrow \text{sampleNeighbors}(G, V_{next})
end while
S.\mathsf{pushBack}(V_e)
\Gamma \leftarrow \operatorname{getInitialPath}(G, S)
\mathcal{B} \leftarrow \operatorname{getCorridor}(\Gamma)
\mathcal{P} \leftarrow \text{sampleViaPoints}(\mathcal{B})
\tau^h \leftarrow \text{trajectoryPlanning}(p_{start}, p_{end}, \mathcal{B}, \mathcal{P}, \delta)
```

is generated and the robot moves along this trajectory. Once the length of the historical path buffer reaches \mathcal{H}^h , the path replanning module (Alg. 1) is periodically executed at interval T. At each step, the agent determines whether to trigger replanning and, if so, how to construct the intention domain. If no feasible path is found within the intention domain, the robot halts and remains in the same state until a feasible action is obtained. The maximum episode length is limited based on the size of the map.

The reward function consists of three components:

$$R = w_1 r_{task} + w_2 r_{terminal} + r_{req}. (7)$$

In (7), r_{task} encourages the replanned trajectory to align with the human intended path. This reward is inversely proportional to the Euclidean distance error between the next H^r points of the human and robot desired paths. The exponential term normalizes the error to the range [0,1], while a geometric weighting assigns higher importance to points closer to the

robot's current position p:

$$\begin{split} r_{task} &= \frac{1-\lambda}{1-\lambda^{H^r}} \sum_{j=1}^{H^r} \lambda^{j-1} e^j \\ e^j &= \exp(-\eta ||p^r(k^r+j) - p^h(k^h+j)||_2) \\ k^i &= \operatorname{argmin}_{1 \leq k \leq |\tau^i|} ||p^i(k) - p||, \quad i = \{r, h\}. \end{split} \tag{8}$$

The term $r_{terminal}$ is a sparse reward: it penalizes the agent when an invalid intention domain is produced and provides a positive reward when the robot reaches the final goal:

$$r_{terminal} = \begin{cases} +1, & \text{if final goal reached} \\ -1, & \text{if intention domain invalid} \\ 0, & \text{otherwise.} \end{cases}$$
 (9)

The weights w_1 and w_2 balance the contributions of the task reward and the terminal reward. Finally, r_{reg} is a regularization reward that constrains the geometric shape of the intention domain:

$$r_{reg} = \begin{cases} \beta \frac{\ln(1 - \phi_{norm})}{1 - \phi_{norm}}, & \text{if } r_{reg} \ge -w_2 \\ -w_2, & \text{otherwise.} \end{cases}$$
 (10)

When the cone base overlaps with obstacles, enlarging the base radius no longer affects the sub-goals; thus, wider cone angles are penalized. The penalty increases with the normalized half-opening angle ϕ_{norm} and is scaled by parameter β , but its magnitude is bounded by $-w_2$ to maintain training stability.

IV. LOCALLY SHARED CONTROLLER

In contrast to the training process, in real interactions the agent does not need to trigger path replanning when the robot's intended path is already consistent with the human's intention. To accommodate such interventions while maintaining safety, we implement a locally shared controller, drawing inspiration from shared DWA [39].

The Dynamic Window Approach (DWA) [40] remains one of the most widely used methods for local obstacle avoidance in mobile robot navigation. By sampling candidate velocity commands within the dynamic velocity window and minimizing a multi-objective cost function, DWA enables safe, smooth, and goal-directed motion in unstructured environments. To adapt DWA for shared control, prior works [39] modify the cost function to incorporate user input. Following this idea, we design a switched local controller. When the operator provides no input, the controller defaults to a standard DWA planner. When the operator issues a command, the controller first evaluates its feasibility by computing clearance, defined as the distance from the terminal point of the commanded trajectory to the closest obstacle. If the clearance exceeds a predefined threshold, the optimal action is chosen by minimizing a modified cost function:

$$C = 1 - Clearance + Clearance \cdot Cost_{cmd}$$

$$Cost_{cmd} = 0.5 \cdot Heading + 0.5 \cdot Velocity$$
(11)

where the Heading term measures how well the curvature fits the human target curvature, and the Velocity term assesses how close the linear speed v is to the user's desired linear speed v^h . All cost terms are normalized to [0,1].

TABLE I
EVALUATION WITH GENERATED HUMAN TRAJECTORIES. RESULTS ARE
AVERAGED OVER THREE RUNS WITH DIFFERENT RANDOM SEEDS.

Model	e_{MED} (m)	f	2φ (°)
baseline	1.32 ± 0.06	1.00	-
$\beta = 0.0$	0.96 ± 0.11	0.29 ± 0.04	92.41 ± 7.76
$\beta = 0.1$	0.97 ± 0.12	0.27 ± 0.03	69.18 ± 6.22
$\beta = 0.5$	$\textbf{0.88}\pm\textbf{0.11}$	0.20 ± 0.03	56.22 ± 6.64
$\beta = 2.0$	0.93 ± 0.12	0.17 ± 0.03	33.46 ± 5.98

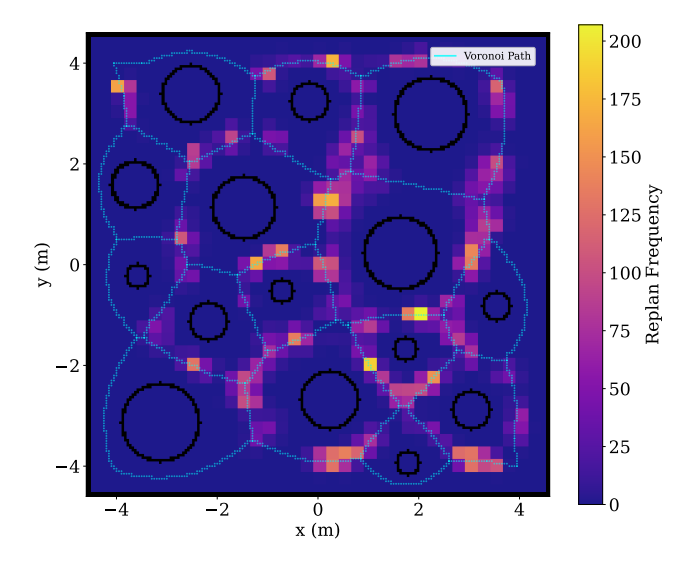


Fig. 4. Heat map visualization of the distribution of replanning trigger locations, evaluated over 256 human-desired trajectories. The discretized Voronoi diagram is overlaid in green lines.

V. SIMULATIONS

To simulate a cluttered environment, we randomly generate a 10m×10m grid map with non-overlapping circular obstacles. The coordinate origin is set at the map center, with the start and goal positions at (-4.0, -4.0) and (4.0, 4.0), respectively. Human desired trajectories are produced using Alg. 2 with a sampling interval of $\delta = 0.1 \,\mathrm{s}$ and employed for model training. The low-level control period matches the trajectory sampling interval, while the high-level decision period is set to T=0.5 s. The egocentric map has a width of W=5 m; the observation horizon of robot intention and the length of the historical buffer are $H^r = 100$ and $H^h = 20$, respectively. Both the policy and value functions are approximated by threelayer fully connected neural networks with 512, 256, and 128 neurons. The reward function employs $\eta = 1.0$ and $\lambda = 0.98$, with corresponding weights $w_1 = 2$ for the task reward and $w_2 = 10$ for the terminal reward. The model is trained for a total of 2×10^7 time steps.

A. Evaluation with Generated Human Trajectories

In this experiment, we compare our methods with a commonly used path replanning method, continually triggered baseline, to validate we can reduce the times of triggering replanning and also reduce the prediction error between robot desired path and humen intention by intention domain prediction and trigger policy learning. The continually triggered baseline performs replanning at every high-level decision

interval, producing a new trajectory from the robot's current position to the final goal. This method is widely adopted in mobile robot navigation systems to cope with unpredictable or dynamic environments. Additionally, we evaluate the effect of the parameter $\beta \in [0, +\infty)$ in the regularization reward term (10) on policy. To better understand the learned path replanning strategy, we also examine the spatial distribution of replanning trigger positions across the map.

Since no human operator is involved, the robot autonomously follows the generated human-desired trajectories. To comprehensively capture global trajectory uncertainty, all simple paths connecting the start and goal nodes are extracted from the Voronoi graph. Following on Alg. 2, looped trajectories are then generated with the same forward and reverse paths. This procedure produces 256 human desired trajectories in total.

For each trajectory, the Mean Euclidean Distance (MED) between the robot's desired and human desired paths is computed to evaluate prediction error e_{MED} . As the robot performs periodic path replanning, MED is calculated over the next H_r points at each decision step and averaged across the entire run. Furthermore, we record the average replanning frequency f, defined as the ratio of triggered replanning events to total decision steps, and the average opening angle 2ϕ of the predicted intention domains. Final results are reported as the mean values over all trajectories.

Table I summarizes the quantitative results. Compared with the baseline, our method greatly reduces the replanning frequency while achieving lower trajectory prediction errors, indicating that the predicted intention domain effectively captures the operator's motion intention over time. The lower replanning frequency also suggests that our approach can recognize local uncertainties in the human's intended trajectory and maintain stable robot behavior despite operator noise or minor interventions, thereby reducing feedback frequency and improving communication efficiency.

As β increases, both the replanning frequency and the opening angle of the intention domain decrease, demonstrating that the triangular regularization reward effectively shapes the replanning strategy. Therefore, if the operator's current heading is considered more important than global goal information during prediction, to increase β yields a smaller opening angle, making the replanned trajectory more aligned with the human's current direction. According to the Table I, $\beta=0.5$ produced the lowest average prediction error and was therefore used in subsequent evaluation.

Fig. 4 illustrates the distribution of replanning trigger locations for the model with the lowest prediction error, evaluated over 256 human-desired trajectories. Replanning is rarely triggered when the robot is near Voronoi nodes but becomes more frequent along edges. This occurs because, at nodes, the agent faces high global and local uncertainty regarding the human's intended direction, whereas along edges, reduced global uncertainty and surrounding obstacles make the operator's future movement more predictable. Additionally, in regions close to obstacles, the probability of triggering replanning is also relatively low. This is because the waypoints used to generate training trajectories are sampled from Gaussian

TABLE II
EVALUATION RESULTS WITH HUMAN IN THE LOOP UNDER THREE
DIFFERENT SUBGOAL DISTRIBUTIONS.

Case	Condition	T_{total} (s)	ρ	D_{clear} (m)
(a)	HL SC	31.0467 33.8700	97.65% 24.22 %	0.5421 0.6090
(b)	HL SC	34.9400 38.8333	98.39% 39.59 %	0.5400 0.5445
(c)	HL SC	64.3467 67.3800	98.91% 51.10%	0.5490 0.5802

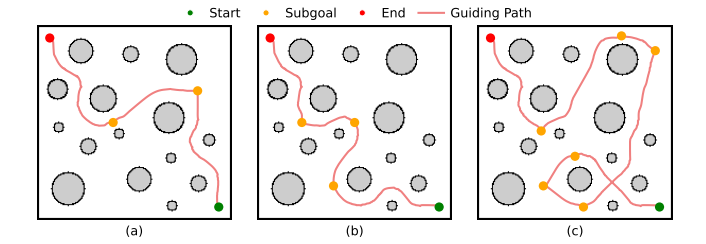


Fig. 5. Visualization of three subgoal distribution scenarios.

rather than uniform distributions, reducing the likelihood of trajectories that closely follow obstacle boundaries.

B. Evaluation with Human in The Loop

To rigorously analyze the behavior of the agent in a controlled and repeatable setting, human in the loop simulations were performed. A simulation world was constructed in Gazebo based on the occupancy grid map shown in Fig. 5, using the same start and goal positions as in the prior experiment. The robot was TurtleBot3. Localization was achieved through the Nav2 framework [41]. The human operator controlled the robot via a joystick. As shown in Fig. 6, the monitoring interface displayed both the front camera view (left) and the occupancy grid map (right). The camera view enabled the operator to identify sub-goal positions, while the map provided visualization of the robot's current planned trajectory.

To represent diverse human intentions, three sub-goal distributions were defined (Fig. 5). And to inform the operator the distributions of sub-goals, a guiding path connecting all sub-goals sequentially from start to goal was overlaid on the occupancy grid map. This design explicitly conveyed the intended route to the operator, ensuring consistent motion intent during evaluation.

To further verify the effectiveness of our approach in reducing operator effort without compromising task efficiency, we adopted the shared DWA algorithm as a baseline, which requires direct human control. Under this method, the robot assists the operator in obstacle avoidance but does not perform autonomous motion planning. For our method, the policy with the lowest prediction error, as reported in Table I, was selected for this experiment. Algorithm performance was evaluated using the following objective metrics:

- 1) Completion time T_{total} : total time required to reach the final goal.
- 2) **Interaction percent** ρ : proportion of total task duration during which the human provided control input.

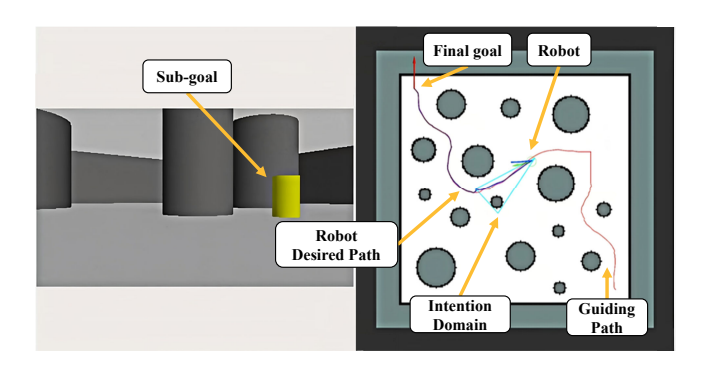


Fig. 6. Monitor interface in simulation. Left: the robot's front camera view. Right: the occupancy grid map with the robot's desired trajectory, final goal and guiding path.

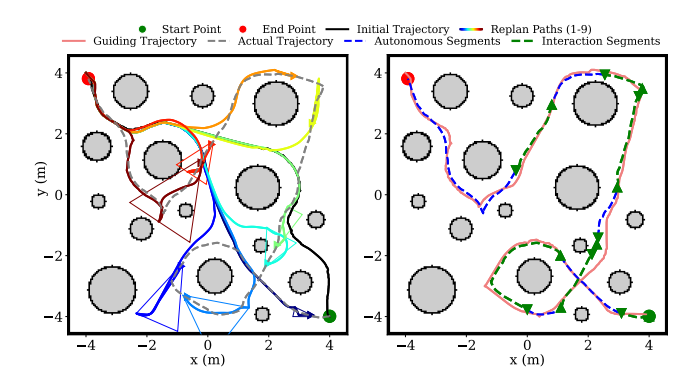


Fig. 7. Left: Replanned paths and corresponding intention domains from one representative experiment (nine in total). Right: Actual versus guiding trajectory, with human-intervened segments shown in green.

3) **Trajectory clearance** D_{clear} : average distance from each trajectory point to the nearest obstacle.

As shown in Table II, under all three sub-goal distributions, the interaction percent decreased significantly. Although the interaction rate increased slightly with the number of subgoals, our method still reduced nearly half of the human effort in the most complex case (c). Additionally, the trajectory safety improved consistently under all conditions. The result demonstrates that the proposed shared control method effectively reduce the operator's workload and enhances safety. A slight increase in task completion time was observed in all three cases. This can be attributed to two factors: first, the experimenter conducting data collection was already proficient in manually controlling the robot within this map; second, operators required additional time to perceive and evaluate the robot's replanned trajectories. Therefore, as task conditions become more demanding, such as in cluttered environments or tasks with higher control complexity, the advantages of the proposed method are expected to become even more

To better understand the path replanning strategy, we visualized the full cooperation process between the human and robot from a representative experiment under one subgoal distribution case (Fig. 5 (c)).

As shown in Fig. 7, the gray dashed line represents the actual motion trajectory, while the black solid line denotes the robot's initially planned path. Fig. 7(a) illustrates the nine replanning events during the experiment along with their

corresponding intention domains. Among them, the second, sixth, and eighth replanned paths did not change the homotopy relationship of the future trajectory with respect to obstacles. This is because these triggers occurred in relatively open areas, where the local uncertainty of the human's intended trajectory was greater, leading the agent to focus more on the operator's motion tendency during replanning. Moreover, from the third, fourth, and fifth replanning results, it can be observed that when multiple homotopically distinct trajectories were available, the agent tended to select the one with the shortest overall length. This behavior is related to our trajectory generation strategy: since no high-quality human trajectory data were available, shorter paths had a higher probability of being generated by Alg. 2. Subfigure (b) compares the actual motion trajectory with the guiding path, marking the segments where human interventions occurred. It can be observed that in open regions, the operator intervened more frequently, whereas in narrow spaces, control authority could be safely delegated to the robot.

To study whether our approach has a practical impact on usability and efficiency for real users, we conducted a user study using a real mobile robot with human subjects.

VI. USER STUDY ON REAL ROBOT

We conducted a within-subject study on a "search and rescue" task. Ten participants (1 female, 9 males), aged between 21 and 25 years (mean age 23.4), took part in the study. Consistent with the simulation experiments, performance was compared against the shared DWA baseline.

Fig. 8 illustrates the experimental setup. The experiments were conducted an indoor area of approximately $5m \times 5m$. To simulate a search-and-rescue scenario, six candidate subgoal locations were arranged around foam-box obstacles. At the start of each trial, three of these locations were randomly selected, and blue-striped cylindrical markers were placed near the obstacle edges to indicate subgoals. Participants operated a TurtleBot 4 Lite robot via an Xbox controller, guiding it from the start position to sequentially locate and identify the three subgoals before reaching the final goal. The user interface was identical to that used in the simulation study: the left panel displayed the front camera view for subgoal detection, and the right panel showed the occupancy grid map, robot desired trajectory, and task progress. The control algorithm ran on ROS 2 on a workstation equipped with an Intel i7-10710U CPU (1.10 GHz) and 7.7 GiB RAM, communicating with the robot via Wi-Fi. The Nav2 framework [41] was employed to handle perception, localization, planning, and control, while organizing higher-level shared control behaviors within the robot system. During model training, the regularization reward parameter $\beta = 0.5$ was used, with all other settings identical to the simulation experiment.

Prior to the experiment, participants viewed an instructional video that introduced the task procedure and explained the two control methods. They were then guided to the test place to familiarize themselves with the obstacle layout and the potential subgoal locations. After that, they completed a simple search task containing only one subgoal to practice teleoperating the robot. During the formal experiment, every participant



Fig. 8. Physical experimental setup. Left: Experimental environment with the robot performing a search-and-rescue task. Right: The operator remotely controlled the TurtleBot 4 using an Xbox controller while monitoring the environment.

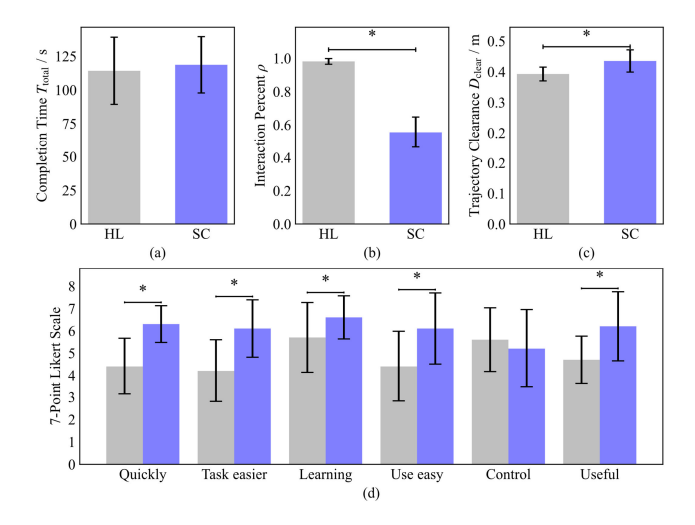


Fig. 9. Results of the user study. Each figure shows the mean and standard error of the different evaluated measures for the two control methods, where * indicates p < 0.05, ** indicates p < 0.01, and *** indicates p < 0.001. (a) The completion time. (b) The interaction percent. (c) The trajectory clearance. (d) The subjective measures.

conducted one preliminary and three recorded trials under each control condition. The order of testing the two methods was randomized across participants to counterbalance novelty and learning effects. After completing the experiment, participants provided subjective ratings of the following usefulness and ease-of-use statements using a seven-point Likert scale.

- 1) "This algorithm helped me complete the task quickly."
- 2) "This algorithm made it easy to complete the task."
- 3) "Learning to use this algorithm is easy for me."
- 4) "I felt in control while using this control method."
- 5) "I would find this control method easy to use."
- 6) "If were to teleoperate a mobile robot, this control method would be useful for me."

We also evaluated the performance of two methods using objective measures mentioned in Section V-B.

For every participant, the mean values of performance metrics were calculated across all three recorded trials under both control conditions. To statistically assess the impact of the proposed shared control framework, paired t-tests with a significance level of $\alpha=0.05$ were performed on task completion time, interaction proportion, and trajectory clearance. The subjective evaluation results were analyzed using the Wilcoxon signed-rank test.

As shown in Fig. 9(a), the completion times was 114.16 \pm 24.87 s for HL condition and 118.59 \pm 20.87 s for

SC condition. Although participants using SC took slightly longer, the difference was not statistically significant $(t(9) = -0.842, \ p = 0.421)$, indicating that proposed shared control method did not compromise task efficiency.

As shown in Fig. 9(b), the interaction percent for the SC condition, $55.48 \pm 9.25\%$, was significantly lower than that for HL, $98.1 \pm 1.71\%$ (t(9) = 14.664, p < 0.001). This result demonstrates that extending shared control to the planning level effectively reduces the operator's workload. Also, this suggests proposed shared control method provides meaningful assistance for robot motion control through intention-aware path replanning.

As shown in Fig. 9(c), the trajectory clearance for the SC condition, 0.43 ± 0.03 m, was significantly $(t(9)=-3.110,\ p=0.013)$ greater than that for HL, 0.39 ± 0.02 m, suggesting that proposed shared control method improves the system safety in cluttered environments.

Regarding subjective measures are summarized in Fig. 9(d). Significant differences were observed between HL and SC for all statements except those related to control and ease of use. Notably, participants rated HL higher than SC in terms of perceived control. These findings indicate that users felt the shared control method helped them complete tasks more efficiently, made operation easier, and provided useful assistance. However, they felt less in control when using SC. This may be because the proposed method requires fully transferring control authority to the robot. In addition, during this user study, participants had only a single trial to become familiar with the shared control method, and the limited interaction opportunities constrained their understanding of the agent's replanning strategy.

VII. CONCLUSION

In this paper, we proposed a novel shared control framework for mobile robots. To reduce the operator's control burden, we extend shared control to the planning level, enabling the robot to infer the operator's motion intention in real time and adjust its desired trajectory accordingly. To achieve intention-aware and safe trajectory adjustment, we proposed a path replanning algorithm based on intention domain prediction. We formulate intention domain prediction and path replanning jointly as a Markov Decision Process and solve it using reinforcement learning. Both simulation and real world experiments were conducted. In simulation, we analyzed the characteristics of the learned replanning strategy and verified its effectiveness in reducing operator workload and improving system safety. In real-world experiments, we performed a user study, and statistical analysis showed that our method significantly reduced operator workload and improved safety without compromising task efficiency.

According to subjective feedback, some participants reported a reduced sense of control when using the proposed method. This may be because limited interaction during the experiments prevented users from fully understanding the agent's replanning strategy. In future work, we plan to investigate how to better evaluate and enhance users' understanding of robot collaboration strategies in shared control tasks, and explore possible improvements to increase user engagement and trust.

REFERENCES

- J. Jiang, P. Di Franco, and A. Astolfi, "Shared Control for the Kinematic and Dynamic Models of a Mobile Robot," *IEEE Transactions on Control* Systems Technology, vol. 24, no. 6, pp. 2112–2124, 2016.
- [2] M. Gao, J. Oberlander, T. Schamm, and J. M. Zollner, "Contextual task-aware shared autonomy for assistive mobile robot teleoperation," in 2014 IEEE/RSJ International Conference on Intelligent Robots and Systems (IROS 2014). IEEE, 2014, pp. 3311–3318.
- [3] D. P. Losey and M. K. O'Malley, "Trajectory Deformations From Physical Human-Robot Interaction," *IEEE Transactions on Robotics*, vol. 34, no. 1, pp. 126–138, 2018.
- [4] Z. Lei, B. Y. Tan, N. P. Garg, L. Li, and A. Sidarta, "An Intention Prediction Based Shared Control System for Point-to-Point Navigation of a Robotic Wheelchair," *IEEE Robotics and Automation Letters*, vol. 7, no. 4, pp. 8893–8900, 2022.
- [5] E. Ng, Z. Liu, and M. Kennedy, "It Takes Two: Learning to Plan for Human-Robot Cooperative Carrying," in 2023 IEEE International Conference on Robotics and Automation (ICRA). IEEE, 2023, pp. 7526–7532.
- [6] Ng, Eley and Liu, Ziang and Kennedy, Monroe, "Diffusion co-policy for synergistic human-robot collaborative tasks," *IEEE Robotics and Automation Letters*, vol. 9, no. 1, pp. 215–222, 2024.
- [7] S. Udupa, V. R. Kamat, and C. C. Menassa, "Shared autonomy in assistive mobile robots: A review," *Disability and Rehabilitation: Assistive Technology*, vol. 18, no. 6, pp. 827–848, 2023.
- [8] C. Masone, M. Mohammadi, P. Robuffo Giordano, and A. Franchi, "Shared planning and control for mobile robots with integral haptic feedback," *The International Journal of Robotics Research*, vol. 37, no. 11, pp. 1395–1420, 2018.
- [9] C. M. El Bou, M. Focchi, M. R. Chang, M. Camurri, and K. D. Von Ellenrieder, "Smooth Human-Robot Shared Control for Autonomous Orchard Monitoring With UGVs," *IEEE Transactions on Automation Science and Engineering*, vol. 22, pp. 13603–13620, 2025.
- [10] J. Li, C. Yang, L. Ding, B. You, and W. Li, "Trilateral Shared Control of a Dual-User Haptic Tele-Training System for a Hexapod Robot With Adaptive Authority Adjustment," *IEEE Transactions on Automation Science and Engineering*, vol. 22, pp. 4366–4381, 2025.
- [11] M. Coffey and A. Pierson, "Collaborative Teleoperation with Haptic Feedback for Collision-Free Navigation of Ground Robots," in 2022 IEEE/RSJ International Conference on Intelligent Robots and Systems (IROS). IEEE, 2022, pp. 8141–8148.
- [12] M. Coffey, D. Zhang, R. Tron, and A. Pierson, "Reactive and Safe Co-Navigation with Haptic Guidance," in 2023 IEEE/RSJ International Conference on Intelligent Robots and Systems (IROS). IEEE, 2023, pp. 213–220.
- [13] Y. Li, R. Cui, W. Yan, C. Feng, and S. Zhang, "Mitigating Over-Assistance in Teleoperated Mobile Robots via Human-Centered Shared Autonomy: Leveraging Suboptimal Rationality Insights," *IEEE Robotics and Automation Letters*, vol. 10, no. 1, pp. 460–467, 2025.
- [14] M. Ma and L. Cheng, "A Human-Robot Collaboration Controller Utilizing Confidence for Disagreement Adjustment," *IEEE Transactions on Robotics*, vol. 40, pp. 2081–2097, 2024.
- [15] D. Sirintuna, A. Giammarino, and A. Ajoudani, "An Object Deformation-Agnostic Framework for Human-Robot Collaborative Transportation," *IEEE Transactions on Automation Science and Engi*neering, vol. 21, no. 2, pp. 1986–1999, 2024.
- [16] G. Hoffman, T. Bhattacharjee, and S. Nikolaidis, "Inferring Human Intent and Predicting Human Action in Human-Robot Collaboration," Annual Review of Control, Robotics, and Autonomous Systems, vol. 7, no. 1, pp. 73–95, 2024.
- [17] J.-A. Yow, N. P. Garg, and W. T. Ang, "Shared Autonomy of a Robotic Manipulator for Grasping Under Human Intent Uncertainty Using POMDPs," *IEEE Transactions on Robotics*, vol. 40, pp. 332–350, 2024.
- [18] L. Han, J. Zhang, and H. Wang, "Shared Control in pHRI: Integrating Local Trajectory Replanning and Cooperative Game Theory," *IEEE Transactions on Robotics*, vol. 41, pp. 1263–1277, 2025.
- [19] S. Luo, M. Cheng, R. Ding, F. Wang, and B. Xu, "Human-Robot Shared Control Based on Locally Weighted Intent Prediction for a Teleoperated Hydraulic Manipulator System," *IEEE/ASME Transactions* on Mechatronics, vol. 27, no. 6, pp. 4462–4474, 2022.
- [20] L. Meng, L. Yang, and E. Zheng, "Hierarchical Human Motion Intention Prediction for Increasing Efficacy of Human-Robot Collaboration," *IEEE Robotics and Automation Letters*, vol. 9, no. 9, pp. 7637–7644, 2024.

- [21] X. Gao, L. Yan, G. Wang, and C. Gerada, "Hybrid Recurrent Neural Network Architecture-Based Intention Recognition for Human-Robot Collaboration," *IEEE Transactions on Cybernetics*, vol. 53, no. 3, pp. 1578–1586, 2023.
- [22] P. Franceschi, D. Cassinelli, N. Pedrocchi, M. Beschi, and P. Rocco, "Design of an Assistive Controller for Physical Human-Robot Interaction Based on Cooperative Game Theory and Human Intention Estimation," *IEEE Transactions on Automation Science and Engineering*, vol. 22, pp. 5741–5756, 2025.
- [23] J. E. Domínguez-Vidal and A. Sanfeliu, "Improving Human-Robot Interaction Effectiveness in Human-Robot Collaborative Object Transportation Using Force Prediction," in 2023 IEEE/RSJ International Conference on Intelligent Robots and Systems (IROS). IEEE, 2023, pp. 7839–7845.
- [24] K.-L. A. Yau, Y. Saleem, Y.-W. Chong, X. Fan, and J. M. Eyu, "The Augmented Intelligence Perspective on Human-in-the-Loop Reinforcement Learning: Review, Concept Designs, and Future Directions," *IEEE Transactions on Human-Machine Systems*, vol. 54, no. 6, pp. 762–777, 2024.
- [25] G. Warnell, N. Waytowich, V. Lawhern, and P. Stone, "Deep TAMER: Interactive Agent Shaping in High-Dimensional State Spaces," *Proceedings of the AAAI Conference on Artificial Intelligence*, vol. 32, no. 1, 2018.
- [26] S. Reddy, A. Dragan, and S. Levine, "Shared Autonomy via Deep Reinforcement Learning," in *Robotics: Science and Systems 2018*. Robotics: Science and Systems Foundation, 2018.
- [27] A. Shafti, J. Tjomsland, W. Dudley, and A. A. Faisal, "Real-World Human-Robot Collaborative Reinforcement Learning," in 2020 IEEE/RSJ International Conference on Intelligent Robots and Systems (IROS). IEEE, 2020, pp. 11161–11166.
- [28] S. W. Abeyruwan, L. Graesser, D. B. D'Ambrosio, A. Singh, A. Shankar, A. Bewley, D. Jain, K. M. Choromanski, and P. R. Sanketi, "i-sim2real: Reinforcement learning of robotic policies in tight human-robot interaction loops," in *Conference on Robot Learning*. PMLR, 2023, pp. 212–224.
- [29] A. Rudenko, L. Palmieri, M. Herman, K. M. Kitani, and D. M. Gavrila, "Human Motion Trajectory Prediction: A Survey," *The International Journal of Robotics Research*, vol. 39, no. 8, pp. 895–935, 2020.
- [30] M. L. Puterman, Markov Decision Processes: Discrete Stochastic Dynamic Programming, ser. Wiley Series in Probability and Statistics.

- John Wiley & Sons, Inc, 2009, no. v.414.
- [31] W. Masson, P. Ranchod, and G. Konidaris, "Reinforcement Learning with Parameterized Actions," *Proceedings of the AAAI Conference on Artificial Intelligence*, vol. 30, no. 1, 2016.
- [32] Z. Fan, R. Su, W. Zhang, and Y. Yu, "Hybrid actor-critic reinforcement learning in parameterized action space," in *Proceedings of the 28th International Joint Conference on Artificial Intelligence*, ser. IJCAI'19. AAAI Press, 2019, pp. 2279–2285.
- [33] J. Schulman, F. Wolski, P. Dhariwal, A. Radford, and O. Klimov, "Proximal policy optimization algorithms," *CoRR*, vol. abs/1707.06347, 2017.
- [34] E. Demeester, A. Hüntemann, D. Vanhooydonck, G. Vanacker, and H. Van Brussel, "User-adapted plan recognition and user-adapted shared control: A Bayesian approach to semi-autonomous wheelchair driving," *Autonomous Robots*, vol. 24, no. 2, pp. 193–211, 2008.
- [35] Y. Ren, F. Zhu, W. Liu, Z. Wang, and Y. Lin, "Bubble Planner: Planning High-speed Smooth Quadrotor Trajectories using Receding Corridors," in 2022 IEEE/RSJ International Conference on Intelligent Robots and Systems (IROS). IEEE, 2022, pp. 6332–6339.
- [36] B. Lau, C. Sprunk, and W. Burgard, "Efficient grid-based spatial representations for robot navigation in dynamic environments," *Robotics and Autonomous Systems*, vol. 61, no. 10, pp. 1116–1130, 2013.
- [37] M. Kuderer, C. Sprunk, H. Kretzschmar, and W. Burgard, "Online generation of homotopically distinct navigation paths," in 2014 IEEE International Conference on Robotics and Automation (ICRA). IEEE, 2014, pp. 6462–6467.
- [38] Rösmann, Christoph and Hoffmann, Frank and Bertram, Torsten, "Planning of multiple robot trajectories in distinctive topologies," in 2015 European Conference on Mobile Robots (ECMR), 2015, pp. 1–6.
- [39] P. Inigo-Blasco, F. Diaz-del Rio, S. Vicente Diaz, and D. Cagigas Muniz, "The shared control dynamic window approach for non-holonomic semiautonomous robots," in ISR/Robotik 2014; 41st International Symposium on Robotics, 2014, pp. 1–6.
- [40] D. Fox, W. Burgard, and S. Thrun, "The dynamic window approach to collision avoidance," *IEEE Robotics & Automation Magazine*, vol. 4, no. 1, pp. 23–33, 1997.
- [41] S. Macenski, F. Martin, R. White, and J. Ginés Clavero, "The marathon 2: A navigation system," in 2020 IEEE/RSJ International Conference on Intelligent Robots and Systems (IROS), 2020.